Journal of Molecular Graphics and Modelling 51 (2014) 27–36

Contents lists available at ScienceDirect

Journal of Molecular Graphics and Modelling

journal homepage: www.elsevier.com/locate/JMGM

A single amino acid change humanizes long-chain fatty acid binding and activation of mouse peroxisome proliferator-activated receptor α

Dhawal P. Oswal, Gerald M. Alter, S. Dean Rider Jr., Heather A. Hostetler*

Department of Biochemistry & Molecular Biology, Boonshoft School of Medicine, Wright State University, Dayton, OH 45435, United States

ARTICLE INFO

Article history:
Accepted 16 April 2014
Available online 29 April 2014

Keywords:
PPAR
Transcription factor
Endogenous ligand
Species differences
Fatty acid
Amino acid differences

ABSTRACT

Peroxisome proliferator-activated receptor α (PPARα) is an important regulator of hepatic lipid metabolism which functions through ligand binding. Despite high amino acid sequence identity (>90%), marked differences in PPARα ligand binding, activation and gene regulation have been noted across species. Similar to previous observations with synthetic agonists, we have recently reported differences in ligand affinities and extent of activation between human PPARα (hPPARα) and mouse PPARα (mPPARα) in response to long chain fatty acids (LCFA). The present study was aimed to determine if structural alterations could account for these differences. The binding of PPARα to LCFA was examined through in silico molecular modeling and docking simulations. Modeling suggested that variances at amino acid position 272 are likely to be responsible for differences in saturated LCFA binding to hPPARα and mPPARα. To confirm these results experimentally, LCFA binding, circular dichroism, and transactivation studies were performed using a F272I mutant form of mPPARα. Experimental data correlated with in silico docking simulations, further confirming the importance of amino acid 272 in LCFA binding. Although the driving force for evolution of species differences at this position are yet unidentified, this study enhances our understanding of ligand-induced regulation by PPARα and demonstrates the efficacy of molecular modeling and docking simulations.

1. Introduction

Peroxisome proliferator-activated receptor alpha (PPARα) belongs to the nuclear hormone receptor superfamily of ligand-dependent transcription factors and has emerged as one of the central regulators of nutrient–gene interactions. Structurally similar to other members of the nuclear hormone receptor family, the PPARα protein structure consists of an N-terminal ligand-independent transactivation function (AF-1), a highly conserved DNA binding domain (DBD), a hinge region and the C-terminal ligand binding domain (LBD) containing a ligand-dependent transactivation function (AF-2). The LBD of PPARα constitutes a large hydrophobic ligand-binding pocket (1300–1400 Å^3) that allows interaction with a broad range of natural and synthetic ligands [1,2]. PPARα interacts with a variety of endogenous ligands, including fatty acids and fatty acid metabolites, as well as synthetic compounds such as hypolipidemic fibrate drugs, to regulate cellular processes related to fatty acid metabolism, glucose metabolism, inflammation, differentiation and proliferation [3–6].

While long-chain fatty acids (LCFA) serve as major metabolic fuels and important components of biological membranes, they also play a significant role as signaling molecules and gene regulators in response to food intake and nutritional changes. Recently, we have demonstrated that LCFA and their thioesters (long-chain fatty acyl-CoA; LCFA-CoA) constitute high-affinity endogenous ligands of human PPARα (hPPARα) and mouse PPARα (mPPARα). Such ligand binding induces PPARα conformational changes and increases transactivation, consistent with expectations for an endogenous ligand of a ligand-activated nuclear receptor [7]. Thus, PPARα in conjunction with LCFA and their metabolites could serve to regulate metabolic pathways governing fuel utilization, storage, transport and mobilization. However, we also reported differences in binding affinities and the extent of ligand-induced

Abbreviations: PPARα, peroxisome proliferator-activated receptor alpha; DBD, DNA binding domain; LBD, ligand binding domain; RXRα, retinoid X receptor alpha; LCFA, long-chain fatty acids; LCFA-CoA, long-chain fatty acyl-CoA; mPPARα, mouse PPARα; hPPARα, human PPARα; F272I mPPARα, mutant form of mPPARα that has a Phe to Ile substitution at position 272; 6xhis, polyhistidine tag; PPRE, peroxisome proliferator response element; ACOX, acyl-CoA oxidase.

* Corresponding author at: Department of Biochemistry & Molecular Biology, Boonshoft School of Medicine, Wright State University, 3640 Colonel Glenn Hwy, Dayton, OH 45435, United States. Tel.: +1 937 775 4503; fax: +1 937 775 3730.
E-mail address: Heather.Hostetler@wright.edu (H.A. Hostetler).

http://dx.doi.org/10.1016/j.jmgm.2014.04.006
1093-3263/

transactivation between mPPARα and hPPARα in response to saturated LCFA [7].

Species differences in PPARα-mediated downstream regulation of target genes have been noted previously [8,9]. Human and mouse PPARα proteins promote transcription to a different extent in response to certain hypolipidemic agents and phthalate monoesters [10,11]. Furthermore, it is well established that long-term administration of PPARα agonists result in hepatic cancer in rats and mice – an effect that does not occur in guinea pigs, canines, non-human primates, or even humans [12]. While a single cause for the existence of such differences is highly unlikely, possible explanations include: differences in expression levels of PPARα or differences in PPARα target genes, alternatively spliced or mutant forms of PPARα protein, mutations or polymorphisms in target gene response elements, increased expression of oncogenes and/or inhibition of apoptosis [12–15]. However, transgenic mice that express human PPARα mainly in the liver do not exhibit hepatocarcinogenesis upon administration of PPARα agonists [16,17]. This observation suggests that structural differences in the PPARα protein could be the underlying cause of such species variation.

Comparison of the PPARα amino acid sequence across species, particularly of the LBD, resulted in >90% homology [18]. However it should be noted that a single amino acid change can result in marked alterations in ligand selectivity of nuclear receptors. For example, a single amino acid change in the mouse PPARα-LBD (E282) results in altered activity of the protein [19], and a valine to methionine substitution in human PPARα (V444M) produced PPARδ ligand binding characteristics, resulting in loss of fibrate responsiveness [20]. While we have reported differences in mPPARα and hPPARα in response to saturated LCFA [7], the goal of this study was to explore the mechanisms underlying such divergence. We have used methods including: molecular modeling and in silico docking, mutagenesis, spectrofluorometry, circular dichroism spectroscopy and transactivation studies to identify a single amino acid change at position 272 that is largely responsible for the altered saturated LCFA binding.

2. Materials and methods

2.1. Molecular modeling simulations

The crystal structure of the ligand binding domain (LBD) of hPPARα complexed with a synthetic agonist (GW409544) was retrieved from RCSB Protein Data Bank (PDB identifier) [2]. This structure was chosen due to the completeness of the crystal structure (no missing amino acid side chains). The apo form of hPPARα-LBD was generated by extracting the ligand (GW409544) from the 1K7L model (using Swiss PDB Viewer, http://www.expasy.org/spdbv/). This structural model was used in all docking simulations. Since the structure of mPPARα has not been crystallized, a homology modeling approach was used to generate the mPPARα-LBD structure. We compared the amino acid sequence of hPPARα to mPPARα and substituted all amino acid residues that were different in the hPPARα-LBD crystal structure. In total, 23 amino acid residues in the hPPARα-LBD were replaced with the corresponding mPPARα residues, followed by energy minimization of the resulting model. This model was used as an initial structure of mPPARα-LBD for all docking simulations. All energy computations were done in vacuo using GROMOS96 43B1 parameters without reaction field, implemented in Swiss PDB Viewer [21]. An energy minimized model of the F272I mPPARα-LBD was also generated using the Swiss PDB Viewer (http://www.expasy.org/spdbv/).

2.2. Molecular docking simulations

In silico docking studies were performed using both AutoDock Vina 1.1.2 [22] and the FlexiDock™ module available on SYBYL®-X 2.0 (Tripos, St. Louis, MO). While AutoDock Vina 1.1.2 allows only the ligand to have flexible/rotatable bonds, the FlexiDock™ module on SYBYL®-X 2.0 permits both protein (sidechains) and ligands to carry flexible/rotatable bonds. For docking with both AutoDock Vina 1.1.2 and FlexiDock™, a search space or putative binding site was defined in a restricted region of the protein. In the present study, the ligand binding pocket was defined based on the experimentally obtained structure of the GW409544 ligand bound to hPPARα-LBD [2]. Once the hPPARα and mPPARα models were energy minimized, docking simulations were conducted using both AutoDock Vina 1.1.2 and FlexiDock™. Docking simulations were first validated using the GW409544 ligand by comparing the X-ray crystal structure 1K7L (hPPARα-LBD + GW409554) with that of the docking output generated for apo-hPPARα with GW409544. Both AutoDock Vina 1.1.2 and FlexiDock™ generated multiple docking poses (differentiated by RMSD relative to the best pose) that were subjected to careful visualization, and only the most energetically favorable conformations were chosen for further analysis.

Docking of LCFA was carried out using both AutoDock Vina 1.1.2 and FlexiDock™. For each binding conformation, the binding energies were calculated using the FlexiDock scoring function based on the Tripos Force Field, as implemented by FlexiDock. The resulting docking conformations were visualized using the PyMOL Molecular Graphics System (Version 1.5.0.4 Schrödinger, LLC) and the program LIGPLOT [23]. In order to determine the volume of each ligand binding pocket, the PVOME algorithm was utilized [24]. Based on the occupancy of GW409544 within the hPPARα ligand binding pocket, the ligand binding pocket was defined using 37 overlapping inclusion spheres. This pocket was visualized using the Visual Molecular Dynamics (VMD) program [25], and volume-grid points near the protein atoms were systematically deleted with a padding variable of 1.09 (radius of a hydrogen atom) or 0.5 (half of a carbon-hydrogen bond length) using POVME [24]. This was followed by volume measurement of the resultant binding pocket. This process was then repeated for mPPARα and F272I mPPARα.

2.3. Chemicals

Fluorescent fatty acid (BODIPY-C16) was purchased from Molecular Probes, Inc. (Eugene, OR). Docosahexaenoyl-CoA and BODIPY C16-CoA were synthesized and purified by HPLC as previously described [26] and found to be >99% unhydrolyzed. Rosiglitazone was generously provided by Dr. Khalid Elased (Wright State University). All other putative ligands were from Sigma–Aldrich (St. Louis, MO).

2.4. Purification of recombinant F272I mutant mPPARα protein

The cloning and purification of wild-type 6xHis-GST-mPPARα has been described [7]. A mutant form of full-length mPPARα (amino acids 1–468) in which the phenylalanine residue at 272 in helix 3 was replaced by isoleucine (F272I; to mimic hPPARα) was used for all experiments presented herein. The F272I mutation was generated by overlap PCR of 6xHis-GST-mPPARα using the following primers: 5′-AAGAGAATCCACGAAGCCTA-3′, 5′-GAAGACAAAGAGGCAGAGGT-CCGAATCTT-3′, 5′-GGACATGCACTGGCAGTGGAAGATTCG-3′ and 5′-CCGGGAGCTGCATGTGTCAGAGG-3′. The PCR product contained internal *Sma* I and *Xho* I sites which were used to replace the 3′ half of wild-type mPPARα in the 6xHis-GST-mPPARα vector with the mutated PCR fragment to produce 6xHis-GST-F272ImPPARα. This plasmid was confirmed by sequencing. The full-length

recombinant mutant F272I mPPARα protein was expressed in Rosetta™2 cells (Novagen, Gibbstown, NJ) and purified as described previously for the wild-type [7]. The protein purity was verified using SDS-PAGE with Coomassie blue staining and immunoblotting. Protein concentrations were estimated by Bradford Assay (Bio-Rad Laboratories, Hercules, CA) and by absorbance spectroscopy using the molar extinction coefficient for the protein.

2.5. Fluorescence based ligand binding assays

The binding affinity of F272I mPPARα to a fluorescent 16 carbon fatty acid analog (BODIPY C16) or its CoA thioester (BODIPY C16-CoA) was determined as described previously for wild-type mPPARα [7]. Based on the binding affinities obtained herein, displacement assays were performed in the presence of BODIPY C16-CoA (110 nM) using non-fluorescent LCFA and LCFA-CoA as described previously [7]. The maximal fluorescence intensity was measured, and the effect of increasing concentrations of naturally occurring non-fluorescent ligands was measured as a decrease in fluorescence. The direct binding of F272I mPPARα to non-fluorescent ligands was also determined by quenching of intrinsic PPARα aromatic amino acid fluorescence as described previously for wild-type mPPARα [7,26]. For all measurements, emission spectra were corrected for background and inner-filter effects were avoided. Changes in fluorescence intensity were used to calculate the dissociation constant (K_d), inhibition constant (K_i) and the number of binding sites (n) as described previously [27].

2.6. Circular dichroism

Circular dichroic spectra of F272I mPPARα (0.6 μM in 600 μM HEPES pH 8.0, 24 μM dithiothreitol, 6 μM EDTA, 6 mM KCl and 0.6% glycerol) were recorded in the presence and absence of LCFA and LCFA-CoA (0.6 μM) with a J-815 spectropolarimeter (Jasco Inc., Easton, MD) as previously described for the wild-type mPPARα [7]. Spectra were recorded from 260 to 187 nm with a bandwidth of 2.0 nm, sensitivity of 10 millidegrees, scan rate of 50 nm/min and a time constant of 1 s. Ten scans per replicate were averaged, and the average spectrum was used to determine the percent composition of α-helices, β-strands, turns and unordered structures with the CONTIN/LL program of the software package CDpro [27,28].

2.7. Mammalian expression plasmids

The pSG5-hPPARα, pSG5mPPARα, pSG5-hRXRα and pSG5-mRXRα plasmids have been described [7]. The F272I mutant mPPARα was amplified from 6xhis-GST-F272I mPPARα using the following primers: 5′-c*ggatcc*accATGGTGGACACAGAGAGCCC-3′ and ctc*ctcgag*TCAGTACATGTCTCTGTAGA-3′. In these primers, lowercase represents nucleotides outside of the PPARα open reading frame and restriction sites are represented in italics. The PCR product was cloned into the pGEM®-T easy vector (Promega Corp., Madison, WI). A *Bam* HI/end-filled *Xho* I F272I mutant mPPARα fragment was subcloned into the *Bam* HI/end-filled *Bgl* II multiple cloning site of pSG5 (Stratagene, La Jolla, CA) to produce pSG5-F272I mPPARα. The reporter construct, PPRE×3 TK LUC was a kind gift of Dr. Bruce Spiegelman (Addgene plasmid #1015) and contained three copies of the acyl-CoA oxidase (ACOX) peroxisome proliferator response element (PPRE) [29].

2.8. Cell culture and transactivation assay

COS-7 cells (ATCC, Manassas, VA) were grown in DMEM supplemented with 10% fetal bovine serum (Invitrogen, Grand Island, NY), at 37 °C with 5% CO_2 in a humidified chamber. Cells were seeded onto 24-well culture plates and transfected with Lipofectamine™ 2000 (Invitrogen, Grand Island, NY) and 0.4 μg of each full-length mammalian expression vector (pSG5-hPPARα and pSG5-hRXRα, pSG5-mPPARα and pSG5-mRXRα, pSG5-F272I mPPARα and pSG5-mRXRα,) or empty plasmid (pSG5), 0.4 μg of the PPRE×3 TK LUC reporter construct, and 0.04 μg of the internal transfection control plasmid pRL-CMV (Promega Corp., Madison, WI) as previously described [27]. Following transfection incubation, medium was replaced with serum-free medium for 2 h, ligands (1 μM) were added, and the cells were grown for an additional 20 h. Fatty acids were added as a complex with bovine serum albumin (BSA) as described [27,30]. Firefly luciferase activity, normalized to *Renilla* luciferase (for transfection efficiency), was determined with the dual luciferase reporter assays system (Promega Corp., Madison, WI) and measured with a SAFIRE^2 microtiter plate reader (Tecan Systems, Inc., San Jose, CA). The clofibrate treated samples in each case, overexpressing both PPARα and RXRα, were arbitrarily set to 1.

2.9. Statistical analysis

Data were analyzed using a one-way ANOVA to evaluate overall significance (SigmaPlot™, Systat Software, San Jose, CA). A Fisher Least Significant Difference (LSD) post hoc test was used to identify individual group differences. The results are presented as mean ± SEM. The confidence limit of $p < 0.05$ was considered statistically significant.

3. Results and discussion

Since its discovery and cloning, PPARα has been shown to be activated by structurally diverse ligands, including the fibrate class of drugs, some herbicides, phthalate monoesters, fatty acids and fatty acid derivatives [3–6,27]. However, a vast array of studies have highlighted species differences not just with respect to gene regulation [8,9], but also in binding or activation of PPARα [10–12]. For example, mouse and human PPARα display differences in ligand binding, activation and physiological responses upon administration of certain hypolipidemic agonists, phthalate monoesters and LCFA [7,10,11]. The present study examines structural differences in the PPARα proteins, which could be an underlying cause of species differences in ligand binding.

3.1. Molecular modeling simulations of hPPARα-LBD and mPPARα-LBD

The X-ray crystal structure of hPPARα is composed of a helical sandwich and a four-stranded β-sheet. The Y-shaped PPARα ligand binding pocket spans between the C-terminal helix 12 (containing the AF-2) and the 4 stranded β-sheet, splitting into 2 arms roughly parallel to helix 3 [2]. In order to investigate the mechanisms underlying differential binding and activation of mouse and human PPARα in response to LCFA, the amino acid sequences of mPPARα and hPPARα were compared. While human and mouse PPARα proteins (468 amino acids) bear approximately 92% sequence identity, there are 35 amino acid differences (Supplementary Fig. 1). In the X-ray crystal structure of hPPARα-LBD employed in this study (1K7L; 267 amino acids), 23 amino acids are different between the hPPARα-LBD and the modeled structure of the mPPARα-LBD. Regardless of this difference in amino acids, when we compared the energy minimized apo forms of hPPARα-LBD and mPPARα-LBD using Swiss PDB Viewer or the PyMOL Molecular Graphics System, there was no significant 3 dimensional structural difference between the two proteins (Cα atoms RMSD < 0.05 Å^3; data not shown). Similarly, no differences were noted in the Ramachandran plots of the two proteins (data not shown). This was consistent with previous data using circular dichroism spectroscopy that

Table 1
Comparison of binding energies (kcal/mol) for mouse and human PPARα-LBD complexed with LCFA ligands.

Ligand	Chain length: double bonds (position)	hPPARα (kcal/mol)	mPPARα (kcal/mol)	F272I mPPARα (kcal/mol)
Palmitic acid	C16:0	−1150	−284	−1089
Palmitoleic acid	C16:1 (*n*-7)	−1149	−1143	−1149
Stearic acid	C18:0	−1153	−298	−1112
Docosahexanoic acid	C22:6 (*n*-3)	−1187	−932	−1039

Binding energies were derived using the FlexiDock™ module available on SYBYL®-X 2.0 (Tripos, St. Louis, MO).

demonstrated no significant differences in the secondary structural content of hPPARα and mPPARα [7].

Supplementary Figure 1 related to this article can be found, in the online version, at http://dx.doi.org/10.1016/j.jmgm.2014.04.006.

3.2. Molecular docking simulations with hPPARα-LBD and mPPARα-LBD

For all docking simulations we utilized both AutoDock Vina [22] and the FlexiDock™ module available on SYBYL®-X 2.0. In order to validate our docking simulations, we compared the energy minimized structure of hPPARα-LBD + GW409544 obtained using our docking approaches to the experimentally obtained X-ray crystal structure of the same [2]. There was no significant difference between the two structures (Cα RMSD < 0.01 Å^3). Furthermore, the orientation of GW409544, as well as the amino acids participating in the interaction between GW409544 and the protein, was quite comparable in the two structures (Supplementary Fig. 2A and B). Thus, this docking protocol was considered suitable for subsequent docking runs. We next simulated the docking of GW409544 to our energy minimized model of mPPARα-LBD. Although there was no significant difference between the RMSD value for the Cα atoms (RMSD < 0.05 Å), the orientation of GW409544 was remarkably different in the hPPARα-LBD and mPPARα-LBD (Supplementary Fig. 2C and D). This was consistent with previous molecular modeling data which reported similar variations in the orientation and position of GW409544 within the ligand binding pockets of mPPARα-LBD and hPPARα-LBD [31]. It was proposed that part of these variances could be attributed to the bulky phenylalanine residue at 272 in mPPARα-LBD (isoleucine in hPPARα-LBD), and that this may cause a large shift in the phenyloxazol arm of GW409544 (Supplementary Fig. 2D).

Supplementary Figure 2 related to this article can be found, in the online version, at http://dx.doi.org/10.1016/j.jmgm.2014.04.006.

Upon validation of the docking parameters, the docking of LCFA to hPPARα-LBD and mPPARα-LBD were examined. Docking of saturated LCFA (palmitic and stearic acids) were preferentially examined, because mPPARα and hPPARα demonstrate differences in the binding to such LCFA [7]. Based on reported crystal structures and structure–activity relationships, most PPARα agonists bind to PPARα with the acidic head group forming hydrogen bonds with Y314 on helix 5 and Y464 on the AF-2 of helix 12. The hydrophobic tails of these ligands are stabilized by numerous hydrophobic interactions extending upward or downward in the 2 arms of the PPARα pocket [2]. Based on these observations and the fact that LCFA serve to activate PPARα, we expected the carboxylic acid group of the LCFA to form a specific hydrogen bonding network with Y314 and Y464 to stabilize the AF-2 helix, permitting PPARα activation.

The binding mode of palmitic acid to hPPARα-LBD demonstrated striking resemblance to that of other PPARα agonists – stabilized by a combination of hydrogen bonds and hydrophobic interactions. The carboxylic acid group of palmitic acid was oriented toward the AF-2 helix forming hydrogen bonds with Y314 and Y464, and its hydrophobic tail was stabilized by numerous hydrophobic interactions in the core PPARα pocket (Fig. 1A and Supplementary Fig. 3A). Similar docking poses were generated for another saturated (stearic acid; C18:0; Supplementary Fig. 4A), monounsaturated (palmitoleic acid; C16:1; Supplementary Fig. 4B) and polyunsaturated (docosohexaenoic acid; C22:6; Supplementary Fig. 4C) LCFA. The binding energies estimated by the docking software are presented in Table 1. Although both AutoDock Vina and the SYBYL®-X 2.0 gave consistent and similar output for the docking modes, the FlexiDock™ module on SYBYL®-X 2.0 was used to obtain binding energies associated with this docking. The FlexiDock™ module on SYBYL®-X 2.0 was chosen because (1) it permits both protein (sidechains) and ligands to carry flexible/rotatable bonds, and (2) the FlexiDock™ energy evaluation function is based on the Tripos Force Field which estimates the binding energy of the ligand, the receptor binding pocket, and the interaction between them. These results demonstrated that LCFA are bound in a similar manner as other PPARα ligands and further support previous observations that suggest LCFA are high affinity endogenous ligands of hPPARα [3,7,27].

Supplementary Figure 3 related to this article can be found, in the online version, at http://dx.doi.org/10.1016/j.jmgm.2014.04.006.

While experimental results indicate that mPPARα binds with strong affinity to monounsaturated and polyunsaturated LCFA, it binds only weakly to saturated LCFA [7]. Consistent to these observations, our docking simulations demonstrated that, with the exception of saturated LCFA, the binding modes and energies generated for the mPPARα-LBD in complex with monounsaturated (C16:1; Supplementary Fig. 4A) and polyunsaturated (C22:6; Supplementary Fig. 4C) LCFA are quite comparable to that of hPPARα-LBD. However, the conformation and position of saturated palmitic (Fig. 1C, Supplementary Fig. 3B) and stearic acid (Supplementary Fig. 4B) in the mPPARα-LBD are remarkably different, demonstrating 4-fold higher binding energies (weaker binding) when compared to the docking poses in hPPARα-LBD (Table 1).

Supplementary Figure 4 related to this article can be found, in the online version, at http://dx.doi.org/10.1016/j.jmgm.2014.04.006.

Two striking features were noted between the binding orientation of palmitic acid and stearic acid to mPPARα-LBD compared to hPPARα-LBD. Although multiple docking poses were generated, suggesting several possible conformations of the palmitic (or stearic) acid within the binding pocket, these characteristics were consistently seen in all poses for the mPPARα-LBD. First, the carboxylic acid group did not form hydrogen bonds with the C terminal amino acids (important for AF-2 interaction) – possibly raising the binding energy (less negative or less favorable). Second, the acyl chain is not fully extended in the mPPARα-LBD pocket (Fig. 1C, Supplementary Fig. 3B), and the fatty acid was unable to orient along the same axis as seen with the hPPARα-LBD. This may raise the binding energy, resulting in weaker binding affinity of saturated LCFA to mPPARα-LBD. It is known that saturated acyl chains normally prefer a fully extended conformation [32]. These results were consistent with the weaker binding affinities of saturated LCFA reported for mPPARα [7]. While the computational and experimental binding

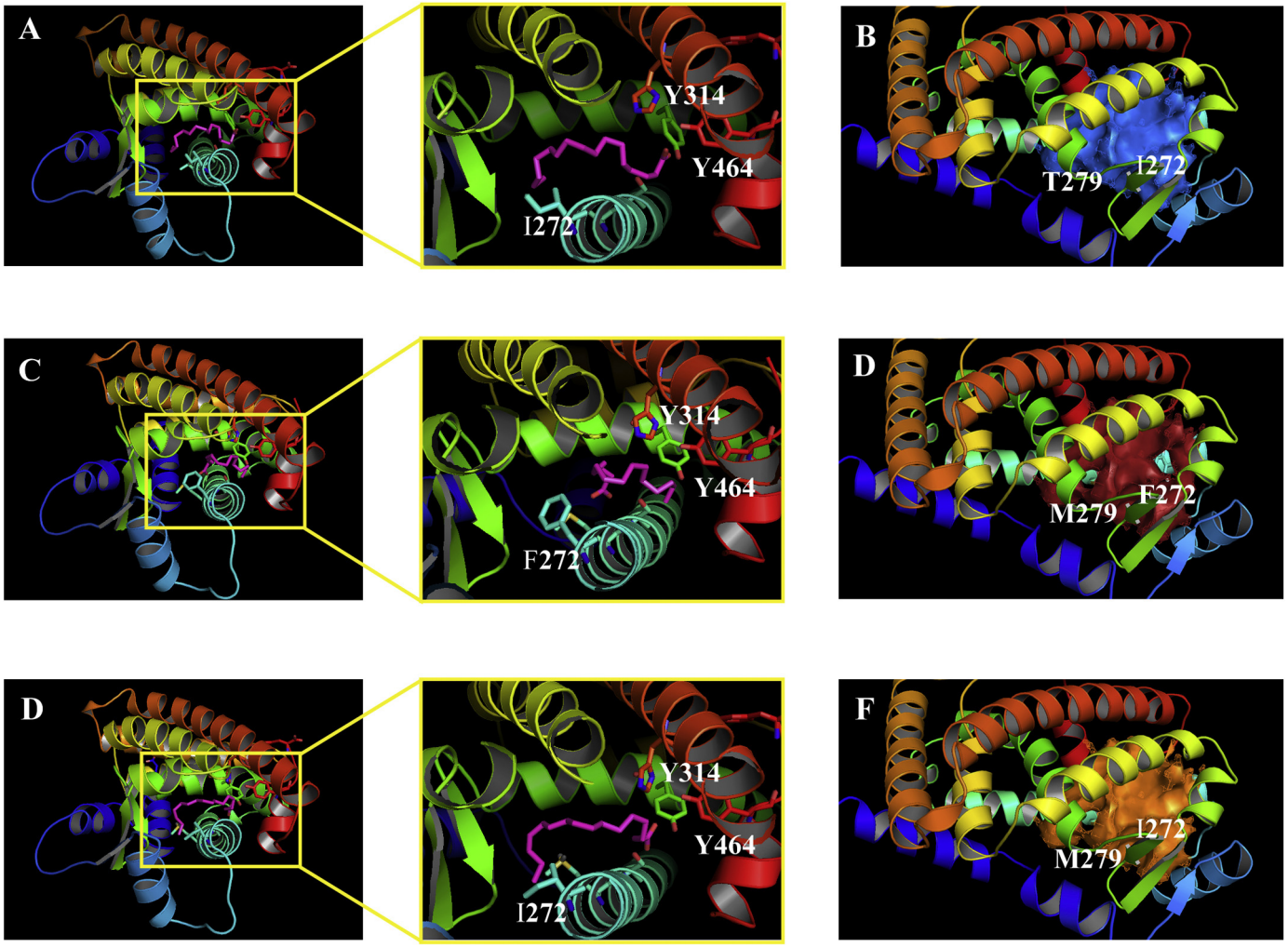

Fig. 1. Comparison of the binding modes of C16:0 complexed with (A) hPPARα-LBD, (C) mPPARα-LBD and (E) F272I mPPARα-LBD. All docking poses presented here were generated using the FlexiDock™ module available on SYBYL®-X 2.0 and are comparable to those generated using AutoDock Vina. In the left-hand figures helix 12, helix 3 and helix 5 are depicted in red, cyan and green respectively. The middle panel figures are close-up views of respective panels from the left. The ligand is colored in magenta and the amino acids Tyr314, Tyr464 and Ile272 or Phe272 are labeled. The figures on the right represent the comparison of the ligand binding cavities of (B) hPPARα-LBD, (D) mPPARα-LBD and (F) F272I mPPARα-LBD. The volumes of the ligand binding pockets were determined to be 1177 Å^3 (hPPARα-LBD; blue), 1073 Å^3 (mPPARα-LBD; red), and 1130 Å^3 (F272I mPPARα-LBD; orange). The amino acid residues at 272 and 279 are labeled.

trends are similar, it is noteworthy that the binding energies obtained in this study do not necessarily convert into the same nanomolar binding affinities reported experimentally. Such differences between computational binding energies and experimental binding affinities could in part be explained by parameters that are not taken into consideration in the docking simulations, including the effect of solvation, contribution of entropy, and the dynamic nature of proteins in solution. However, solvation itself is not likely to account for the large differences in LCFA binding by hPPARα and mPPARα. This is because the solvation energies of palmitic or stearic acid are about the same, regardless of the protein to which they are bound [33]. Further, the hydration of the binding pockets are also estimated to be similar, given the similar polarity of the amino acid substitutions at 272 and 279 (F272I and T279M). However, the overall protein flexibility and the role of water in this process are of particular importance. While these possibilities were not tested in this study, another factor that may play a crucial role in explaining such differences is the use of full-length PPARα protein in experimental ligand binding studies as compared to the use of only the PPARα-LBD in computational docking simulations.

Comparison of the amino acid sequences from the human and mouse PPARα-LBD, especially in helices 3, 5, 7 and 12 which form the central core of the ligand binding pocket, exhibit two major differences in helix 3, which occur at amino acid 272 (isoleucine to phenylalanine) and 279 (threonine to methionine). While both of these substitutions are fairly conservative, the amino acid at 272 in hPPARα is an isoleucine with a small isobutyl group, whereas in mPPARα this residue is a phenylalanine with a bulkier benzyl side chain. We speculated that the electron rich bulkier benzyl group of F272 in mPPARα might cause steric hindrance and change the shape and volume of the mPPARα ligand binding pocket (Fig. 1B and D). In order to test this hypothesis, we substituted the phenylalanine residue at 272 in the mPPARα-LBD structure with an isoleucine (F272I mPPARα-LBD).

The binding modes and energies generated using such an energy minimized model of F272I mPPARα-LBD in complex with palmitic acid (Fig. 1E and Supplementary Fig. 3C), as well as palmitoleic, stearic and docosahexaenoic acids were similar to that obtained using the hPPARα-LBD structure (Table 1). These results suggest that the amino acid residue at position 272 of helix 3 plays a critical role in determining species specificity and selectivity of PPARα ligands. The slight difference in the binding energy between hPPARα-LBD and mPPARα-LBD complexed with C22:6 may be attributed to the manner in which the ligand orients around

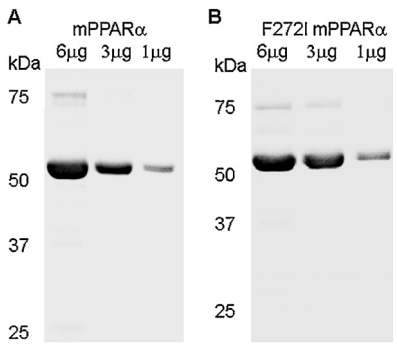

Fig. 2. SDS-PAGE and Coomassie blue staining of 1 μg, 3 μg and 6 μg of purified recombinant (A) mPPARα (left) and (B) F272I mPPARα showing relative purity of the protein. The prominent band at 52 kDa represent full-length, untagged recombinant mPPARα and F272I mPPARα.

the amino acid at 279 (threonine in hPPARα and methionine in mPPARα), although this possibility was not examined. This T279M substitution has previously been reported to cause differences in the activation of human and mouse PPARα in response to synthetic PPARα agonists [34].

To determine the contribution of these amino acids to the PPARα ligand binding pocket, the binding pocket volumes were calculated using the POVME algorithm. Based on the occupancy of the GW409544 ligand (in 1K7L) and a padding variable set to 0.5 (deduced based on a carbon-hydrogen bond length of 1.09 Å), the ligand binding pocket of hPPARα-LBD was 1177 Å^3 (Fig. 1B). In contrast, the binding pocket of mPPARα-LBD was 1073 Å^3 (Fig. 1D). A single mutation of F272I or two mutations including both F272I and M279T in the mPPARα-LBD resulted in binding pocket volumes of 1130 Å^3 (Fig. 1F) and 1161 Å^3 (data not shown), respectively. It is apparent from these results that the amino acid differences at residues 272 and 279 do alter the size of the pocket. However, as the average volume of a fatty acid (e.g. palmitic acid) is <300 Å^3, there is plenty of space within each of these pockets for fatty acid binding. This suggests that favorable interactions with the AF-2 domain (which are based on the orientation of the ligand) are more important for determining PPARα ligand specificity, with regards to LCFA, than the total volume available within the pocket.

3.3. Purification of full-length recombinant F272I mPPARα

In order to experimentally determine the effect of a phenylalanine to isoleucine substitution at amino acid 272 of mPPARα, full-length recombinant F272I mPPARα protein was expressed and purified as described for full-length mPPARα and hPPARα [7]. SDS-PAGE and Coomassie blue staining indicated a predominant band (>90%) of 52 kDa corresponding to the expected size of full-length F272I mPPARα (Fig. 2B), with similar purity as mPPARα (Fig. 2A). In both proteins, a small amount of tagged protein is seen at 75 kDa (Fig. 2).

3.4. Binding of fluorescent fatty acids and fatty acyl-CoAs to F272I mPPARα

While BODIPY fluorescence was low for each examined fluorophore in the absence of protein, titration of F272I mPPARα with BODIPY C16-CoA resulted in increased fluorescence which approached saturation near 200 nM (Fig. 3A and B). This data transformed into a linear double reciprocal plot (Fig. 3B, inset), consistent with a single binding site ($R^2 > 0.90$). Binding of BODIPY C16 fatty acid was also strongly saturable at a single binding site (Fig. 3C). Multiple replicates yielded K_d values of 55 ± 4 nM and 18 ± 3 nM for BODIPY C16-CoA and BODIPY C16 fatty acid, respectively, indicating high-affinity binding. These results were consistent with previously reported binding affinities of wild-type mPPARα [7], suggesting that this amino acid change did not disrupt or alter the binding of these ligands.

3.5. Binding of endogenous LCFA and LCFA-CoA to F272I mPPARα

In order to experimentally test the hypothesis that the F272I substitution could explain the differences in binding affinity of human and mouse PPARα for saturated LCFA, the ligand specificity of F272I mPPARα for naturally occurring, endogenous LCFA and LCFA-CoA was examined. The binding affinities for naturally occurring LCFA and LCFA-CoA were estimated by monitoring their ability to compete and displace BODIPY C16-CoA from F272I mPPARα, which was observed as decreased BODIPY fluorescence. With the exception of lauric acid and lauroyl-CoA, titration with the fatty acids and fatty acyl-CoA examined here resulted in significantly decreased BODIPY fluorescence (Supplementary Fig. 5). Quantitative analyses of these data suggested strong binding (K_i = 17–29 nM, Table 2). By comparison, the synthetic PPARα agonist clofibrate showed slightly weaker binding affinity (K_i = 51 nM), and the synthetic PPARγ agonist rosiglitazone did not displace BODIPY C16-CoA (Supplementary Fig. 5L, Table 2).

Supplementary Figure 5 related to this article can be found, in the online version, at http://dx.doi.org/10.1016/j.jmgm.2014.04.006.

To confirm the ligand binding specificity of F272I mPPARα, the binding affinity of LCFA and LCFA-CoA was also measured by spectroscopically monitoring the quenching of F272I mPPARα aromatic amino acid emission. Titration of F272I mPPARα with both palmitic (Fig. 4A) and stearic (Fig. 4C) acids (saturated LCFA) effectively quenched F272I mPPARα fluorescence, yielding a sharp saturation curve with a maximal change at 100 nM. These data transformed

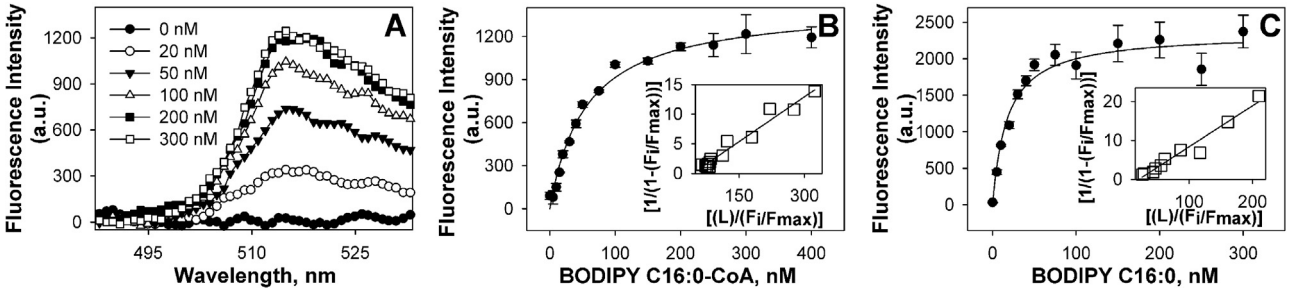

Fig. 3. (A) Corrected fluorescence emission spectra of 0.1 μM F272I mPPARα titrated with 0 (filled circles), 20 (open circles), 50 (filled triangles), 100 (open triangles), 200 (filled squares) and 300 nM (open squares) of BODIPY C16-CoA upon excitation at 465 nm. These results demonstrate increased fluorescence intensity upon binding to F272I mPPARα. Plot of F272I mPPARα fluorescence emission at 515 nm (excitation 465 nm) as a function of BODIPY C16:0-CoA (B) and BODIPY C16:0 FA (C). Insets represent double reciprocal plots of the binding curve from each panel. All values represent the mean ± S.E., $n \geq 3$.

Table 2
Affinity of F272I mPPARα for non-fluorescent ligands determined by quenching of hPPARα aromatic amino acid fluorescence and by displacement of F272I mPPARα-bound BODIPY C16-CoA.

Ligand	Chain length: double bonds (position)	K_d (nM) Fatty acid	K_d (nM) Fatty acyl-CoA	K_i (nM) Fatty acid	K_i (nM) Fatty acyl-CoA
Lauric acid/CoA	C12:0	ND	ND	ND	ND
Palmitic acid/CoA	C16:0	20 ± 3	17 ± 2	19 ± 2	18 ± 2
Palmitoleic acid/CoA	C16:1 (*n*-7)	19 ± 3	21 ± 2	22 ± 3	28 ± 3
Stearic acid/CoA	C18:0	11 ± 2	18 ± 2	15 ± 1	19 ± 2
Docosahexanoic acid/CoA	C22:6 (*n*-3)	17 ± 3	27 ± 3	17 ± 2	29 ± 3
Clofibrate		42 ± 6		51 ± 3	
Rosiglitazone		ND		ND	

Values represent the mean ± S.E. ($n \geq 3$). ND, not determined.

into linear reciprocal plots (Fig. 4A and C insets), indicating high affinity binding at a single binding site (K_d of 20 nM and 11 nM for palmitic and stearic acids, respectively). With the exception of lauric acid (Fig. 4I) and lauryl-CoA (Fig. 4J), similar results were obtained for all examined fatty acids and fatty acyl-CoA (Fig. 4A–H), with single site binding affinities in the 11–27 nM range (Table 2). The PPARα agonist clofibrate strongly quenched F272I mPPARα fluorescence (Fig. 4K), but displayed weaker affinity than the LCFA (Table 2), while the PPARγ agonist rosiglitazone showed no binding (Fig. 4L, Table 2).

While the binding affinities obtained for F272I mPPARα with saturated LCFA were comparable to those obtained with hPPARα (K_d = 14–22 nM), they are significantly different (4–5 fold) from those obtained using wild-type mPPARα (K_d = 81–135 nM, Supplementary Table 1) [7]. These data further corroborate the importance of amino acid residue 272 in determining species selectivity for endogenous PPARα ligands. LCFA-CoA binding was similar to previous reports for both mPPARα and hPPARα [7], suggesting that amino acid 272 is not as important for the orientation of these ligands within the pocket.

Supplementary Table 1 related to this article can be found, in the online version, at http://dx.doi.org/10.1016/j.jmgm.2014.04.006.

3.6. *Effect of endogenous fatty acids and fatty acyl-CoAs on F272I mPPARα secondary structure*

Circular dichroism (CD) was used to examine whether the binding of LCFA or LCFA-CoA altered the F272I mPPARα secondary structure. The far UV CD spectrum of F272I mPPARα suggested the presence of substantial α-helical content, exhibiting a large positive peak at 192 nm and two negative peaks at 207 and 222 nm (Fig. 5A–E, filled circles). Quantitative analyses confirmed that F272I mPPARα was composed of approximately 30% α-helix, 18% β-sheets, 22% β-turns and 29% unordered structures (Table 3). A comparison of the CD spectra (Supplementary Fig. 6) and relative proportions of the secondary structures for wild-type hPPARα, mPPARα and F272I mPPARα suggested no significant differences in the structure of these proteins – a finding consistent with our observations from the modeling data. This suggested that the F272I

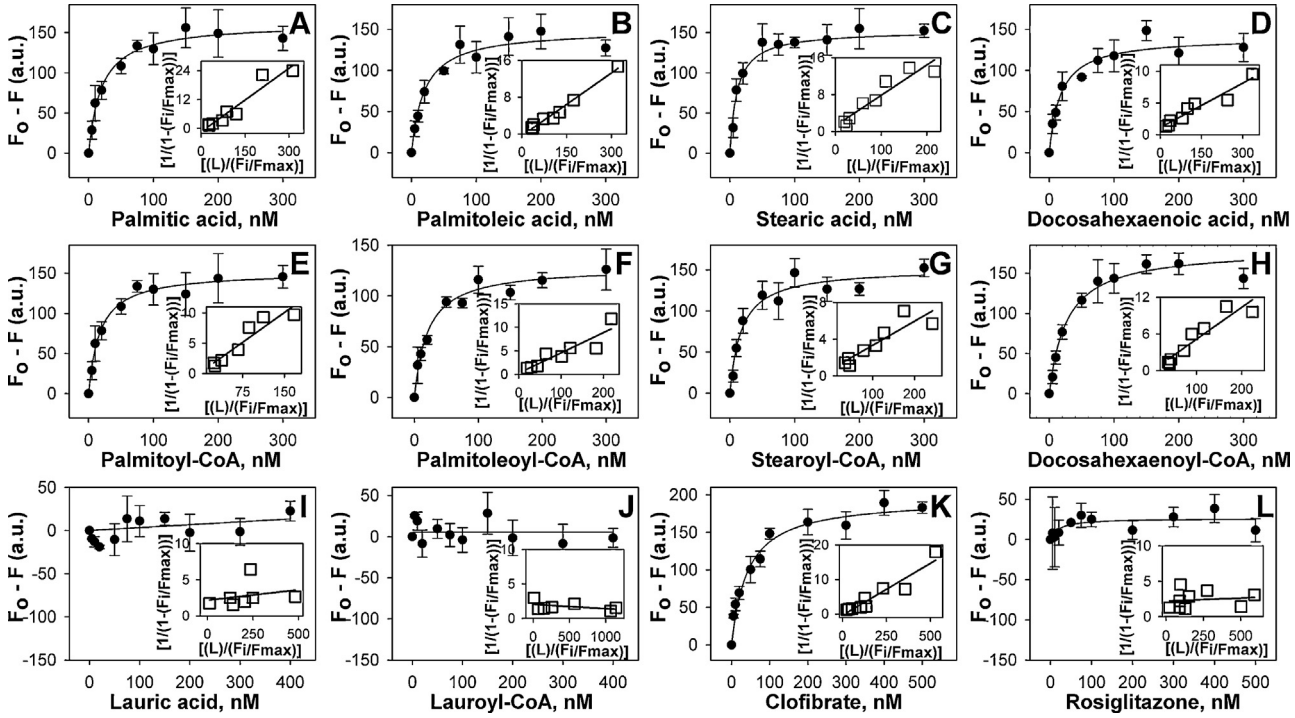

Fig. 4. Interaction of naturally occurring fatty acids and fatty acyl-CoA with F272I mPPARα. Direct binding assay based on quenching of F272I mPPARα aromatic amino acid fluorescence emission (excitation = 280 nm and emission = 300–400 nm) when titrated with the following ligands: (A) palmitic acid, (B) palmitoleic acid, (C) stearic acid, (D) docosahexaenoic acid, (E) palmitoyl-CoA, (F) palmitoleoyl-CoA, (G) stearoyl-CoA, (H) docosahexaenoyl-CoA, (I) lauric acid, (J) lauryl-CoA, (K) clofibrate, and (L) rosiglitazone. Data are presented as the change in fluorescence intensity ($F_0 - F_i$) plotted as a function of ligand concentration. Insets represent linear plots of the binding curve from each panel. All values represent mean ± S.E., $n \geq 3$.

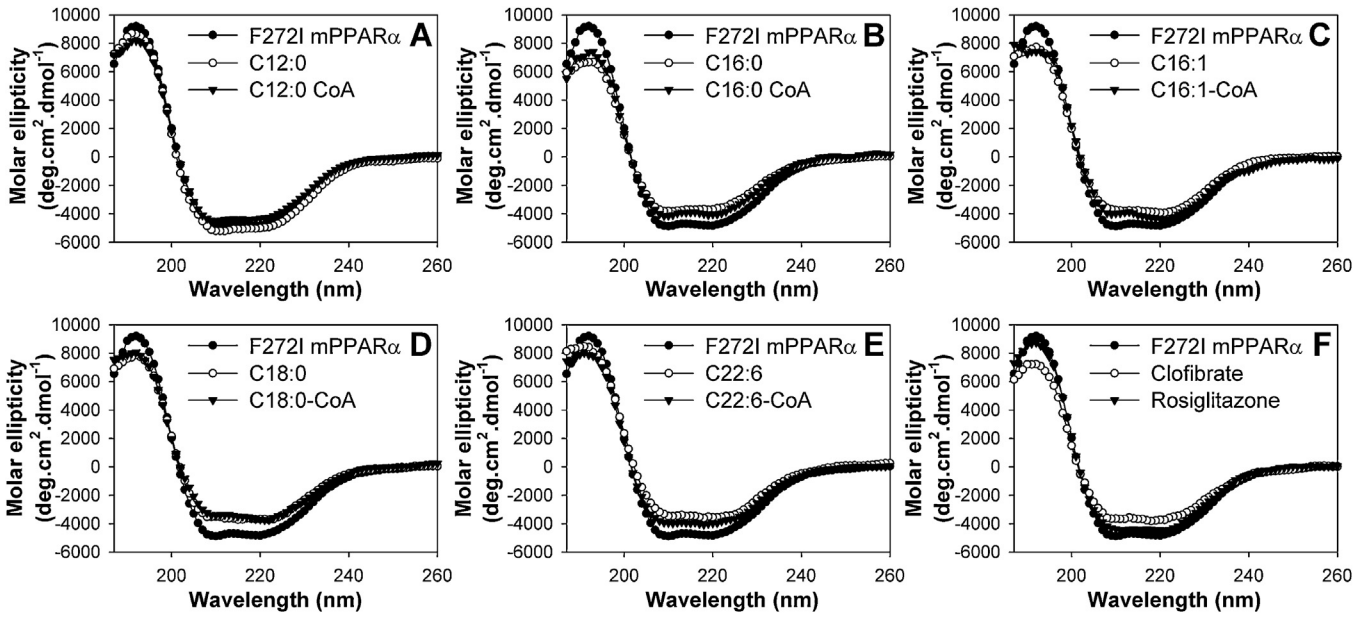

Fig. 5. Far UV circular dichroic (CD) spectra of F272I mPPARα in the absence (filled circles) and presence of added ligand: A, Lauric acid (open circles) or Lauryl-CoA (filled triangles); B, palmitic acid (open circles) or palmitoyl-CoA (filled triangles); C, palmitoleic acid (open circles) or palmitoleoyl-CoA (filled triangles); D, stearic acid (open circles) or stearoyl-CoA (filled triangles); E, docosahexanoic acid (open circles) or docosahexaenoyl-CoA (filled triangles); and F, clofibrate (open circles) or rosiglitzone (filled triangles). Each spectrum represents an average of 10 scans for a given representative spectrum from at least three replicates.

mutation in mPPARα does not disrupt the secondary structure or folding of the protein.

Supplementary Figure 6 related to this article can be found, in the online version, at http://dx.doi.org/10.1016/j.jmgm.2014.04.006.

The addition of high-affinity ligands to F272I mPPARα resulted in conformational changes demonstrated by alterations in the molar ellipticity at 192, 207, and 222 nm (Fig. 5B–E), indicative of ligand binding. Conversely, no changes were observed with the addition of lauric acid (Fig. 5A), lauroyl-CoA (Fig. 5A) or rosiglitazone (Fig. 5F), consistent with the lack of binding of F272I mPPARα to these ligands. While saturated LCFA do not induce secondary structural changes to mPPARα [7], there was a significant decrease in the fraction of α-helical content and a concomitant increase in the fraction of β-sheets for F272I mPPARα (Table 3), similar to those reported for hPPARα [7]. Similar helix-sheet transitions have been previously reported with other nuclear receptors and transmembrane proteins [27,35,36]. Most of the examined LCFA and LCFA-CoA resulted in F272I mPPARα structural changes (Table 3) most similar to those previously reported for hPPARα [7], further indicating the importance of residue 272 in LCFA binding. However, palmitoyl-CoA and docosahexaenoic acid changes (Table 3) were more similar to those reported for mPPARα [7], suggesting that ligand structure may also be important in determining ligand orientation and binding.

3.7. Effect of fatty acids on transactivation of PPARα-RXRα heterodimers

In order to determine whether residue 272 is also responsible for variances observed between mPPARα and hPPARα transactivation in response to saturated LCFA [7], luciferase reporter assays utilizing hPPARα, mPPARα and F272I mPPARα were performed. Since PPARα heterodimerizes with RXRα to induce transactivation, COS-7 cells were cotransfected with either pSG5 empty vector or a combination of hPPARα and hRXRα, mPPARα and mRXRα or F272I mPPARα and mRXRα. The transactivation of a PPRE × 3 TK LUC reporter construct was analyzed in the absence or

Table 3
Effect of ligands on the relative proportion of F272I mPPARα secondary structure determined by CD. These structures were as follows: total helices (H; a sum of regular α-helices and distorted α-helices), total sheets (S; a sum of regular β-sheets and distorted β-sheets), turns (Trn; β-turns), and unordered (Unrd) structures.

Average	Total H ± S.E.	Total S ± S.E.	Trn ± S.E.	Unrd ± S.E.
F272I mPPARα	30 ± 2	18.3 ± 2.3	21.8 ± 0.2	28.8 ± 0.2
F272I mPPARα + lauric acid	29 ± 1	21 ± 2	21.8 ± 0.1	28.9 ± 0.2
F272I mPPARα + lauryl-CoA	30 ± 1	20 ± 1	21.7 ± 0.3	29.1 ± 0.1
F272I mPPARα + palmitic acid	18.1 ± 0.2**	31.5 ± 0.5**	22 ± 0.1	28.6 ± 0.3
F272I mPPARα + palmitoyl-CoA	21 ± 2*	29 ± 1*	22.1 ± 0.3	29.1 ± 0.2
F272I mPPARα + palmitoleic acid	20 ± 1#	30 ± 1#	21.7 ± 0.1	28.7 ± 0.2
F272I mPPARα + palmitoleoyl-CoA	22 ± 2*	28 ± 1*	21.4 ± 0.2	28.5 ± 0.5
F272I mPPARα + stearic acid	18.3 ± 0.1**	31.1 ± 0.1**	21.9 ± 0.1	28.5 ± 0.1
F272I mPPARα + stearyl-CoA	20 ± 1*	29 ± 1*	21.5 ± 0.2	28.7 ± 0.3
F272I mPPARα + DHA	19 ± 1**	30.8 ± 0.3**	21.5 ± 0.1	28.7 ± 0.1
F272I mPPARα + DHA-CoA	19.1 ± 0.1#	30.6 ± 0.3**	22 ± 1	28.6 ± 0.1
F272I mPPARα + clofibrate	17.1 ± 0.1**	31.9 ± 0.3**	22 ± 1	29.0 ± 0.2
F272I mPPARα + rosiglitazone	31 ± 1	19 ± 1	21.9 ± 0.1	28.6 ± 0.1

Asterisks represent significant differences between F272I mPPARα only and F272I mPPARα in the presence of added ligand.
* $P < 0.05$,
** $P < 0.001$ and
# $P = 0.001$.

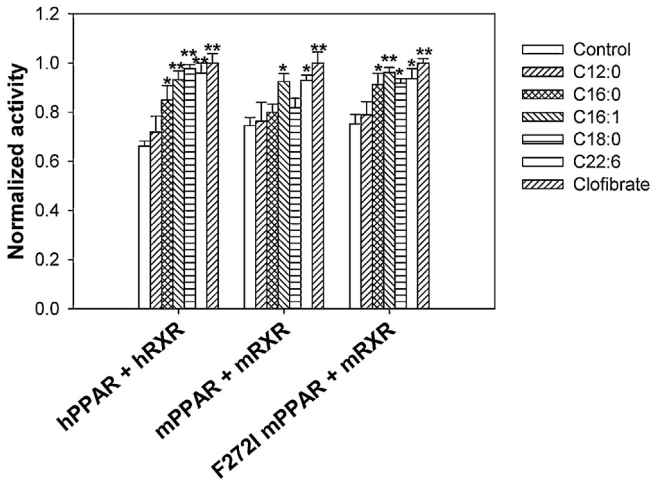

Fig. 6. Fatty acids mediate species-selective transactivation of PPARα-RXRα heterodimers. Cos7 cells transfected with both hPPARα and hRXRα, both mPPARα and mRXRα, or both F272I mPPARα and mRXRα analyzed for transactivation of the acyl-CoA oxidase reporter construct in presence of vehicle (*open bars*), 1 μM lauric acid (*diagonally upward bars*), 1 μM palmitic acid (*hatched bars*), 1 μM palmitoleic acid (*diagonally downward bars*), 1 μM stearic acid (*horizontally lined bars*), 1 μM docosahexanoic acid (*open bars*) and 1 μM clofibrate (*diagonally upward bars*). The *y*-axis represents values for firefly luciferase activity that have been normalized to *Renilla* luciferase (internal control) as well as controls for cells transfected with empty pSG5 vector. The bar graph represents the mean values ($n \geq 3$) ± standard error. $^{*}P < 0.01$, $^{**}P < 0.001$.

presence of ligands (Fig. 6). Transactivation was measured as percent firefly luciferase activity normalized to *Renilla* luciferase (internal control).

Cells overexpressing hPPARα and hRXRα demonstrated significantly increased transactivation of the PPRE × 3 TK LUC reporter in response to high-affinity ligands of hPPARα (Fig. 6). In contrast, for cells overexpressing mPPARα and mRXRα, only the examined unsaturated LCFA and clofibrate significantly increased transactivation. Consistent with the weak binding affinity of saturated LCFA for mPPARα, addition of these ligands did not affect the activity in COS-7 cells. However, in cells overexpressing F272I mPPARα and mRXRα, the addition of saturated LCFA (palmitic and stearic acid), as well as unsaturated LCFA (palmitoleic and docosahexaenoic acid) resulted in significantly increased transactivation, similar to clofibrate-treated cells (Fig. 6). This was consistent with the high-affinity binding of these ligands to F272I mPPARα. In all treatments the addition of lauric acid, which consistently did not bind to hPPARα, mPPARα or F272I mPPARα, had no significant effect on activity. These findings suggested that only high-affinity endogenous ligands increase PPARα activity and, more importantly, the amino acid at 272 could be responsible for the differences in saturated LCFA-mediated transactivation of the PPRE × 3 TK LUC reporter in cells overexpressing hPPARα and mPPARα.

These results are consistent with previous transactivation studies and gene expression studies which demonstrate species differences in the activity of human and mouse PPARα in response to synthetic agonists such as 5, 8, 11, 14-eicosatetraynoic acid (ETYA), WY-14,643 and 2-ethylphenylpropanoic acid derivative (KCL), among others [8–11,34,37,38]. While an I272F substitution diminished the agonistic activity of KCL, a T279 M substitution increased the agonistic activity of WY-14,643 in hPPARα [38]. Our studies with endogenous LCFA ligands suggest that, to a large extent, only amino acid 272 plays an important role in determining species differences, particularly for saturated LCFA. We speculate that based on the structure of ligands and their potential orientation and interactions within the PPARα pocket, both amino acids at 272 and 279 are crucial determinants of species differences exhibited by PPARα across species.

Computational and experimental data support the notion that amino acid substitutions could be responsible for differences in binding affinity and activation observed between human and mouse PPARα. It is believed that during the course of evolution, emerging nuclear receptors acquired the ligand-binding capacities and further refined their specificities for a particular biologically significant ligand [39–41]. Among 117 vertebrate PPARα protein coding sequences identified by BLAST, isoleucine 272 is conserved from bony fish to primates, with the exception of mouse (*Mus musculus*), rat (*Rattus norvegicus*) and two unrelated rodents: the naked mole rat (*Heterocephalus glaber*) and the thirteen-lined ground squirrel (*Ictidomys tridecemlineatus*). The distribution of these species suggests that the substitution of isoleucine for phenylalanine has evolved at least three times. A simple transversion (A to T) in the first position of the codon is enough to convert an isoleucine to a phenylalanine codon. However, given the high evolutionary rate of PPARα [39–41], the conservation of isoleucine in this position implies that there are functional and evolutionary consequences associated with this change (e.g. it is under purifying selection). Consistent with this, our results indicated that compared to humans, the I272F amino acid change seen in mouse represents a partial loss of function mutation (hypomorphic) with respect to LCFA binding. Whether this change is responsible for the increased sensitivity of mouse to peroxisome proliferation or hepatic cancer remains to be determined, but the single F272I substitution in mPPARα recapitulates the human-like LCFA binding and trans-activation functions. Other amino acid positions examined that were not predicted to alter LCFA binding energies (such as position 279) displayed much greater variation among species, suggesting more relaxed functional and evolutionary constraints at those positions.

One could speculate that PPARα underwent strong selective pressure that was directly affected by dietary changes and that this eventually provided crucial structural and functional changes like I272F in mouse. However, there is no clear dietary or metabolic relationship uniquely shared among the four species that harbor the I272F amino acid change, and compensatory mechanisms that may allow this mutation to persist within these species are not clearly established. Therefore, the important question that still remains unsolved is why such differences in PPARα structure would exist.

Nonetheless, we demonstrated for the first time that differences in amino acids in the LBD of PPARα contribute to species selectivity and specificity for endogenous PPARα ligands. The importance of PPARα in human disease is validated by the lipid lowering effects of synthetic PPARα agonists. The data presented herein enhances our understanding of dietary effects on PPARα and may aid in the development of more targeted therapeutics. Moreover, these data demonstrate the efficacy of molecular modeling and docking simulations for examining the effect of structural variations on ligand binding.

Acknowledgements

This work was funded by the National Institute of Diabetes and Digestive and Kidney Diseases NIH Award DK77573 (H.A.H.) and funds from the Boonshoft School of Medicine and the College of Science and Mathematics, Wright State University. The authors would also like to thank Mr. Hemant Purohit for assistance with the POVME algorithm.

References

[1] B. Desvergne, W. Wahli, Peroxisome proliferator-activated receptors: nuclear control of metabolism, Endocr. Rev. 20 (5) (1999) 649–688.
[2] H.E. Xu, M.H. Lambert, V.G. Montana, K.D. Plunket, L.B. Moore, J.B. Collins, J.A. Oplinger, S.A. Kliewer, R.T. Gampe, D.D. McKee, et al., Structural determinants

of ligand binding selectivity between the peroxisome proliferator-activated receptors, Proc. Natl. Acad. Sci. U.S.A. 98 (24) (2001) 13919–13924.
[3] S.A. Kliewer, S.S. Sundseth, S.A. Jones, P.J. Brown, G.B. Wisely, C.S. Koble, P. Devchand, W. Wahli, T.M. Willson, J.M. Lenhard, et al., Fatty acids and eicosanoids regulate gene expression through direct interactions with peroxisome proliferator-activated receptors alpha and gamma, Proc. Natl. Acad. Sci. U. S. A. 94 (9) (1997) 4318–4323.
[4] B.M. Forman, J. Chen, R.M. Evans, Hypolipidemic drugs, polyunsaturated fatty acids, and eicosanoids are ligands for peroxisome proliferator-activated receptors alpha and delta, Proc. Natl. Acad. Sci. U. S. A. 94 (9) (1997) 4312–4317.
[5] M. Rakhshandehroo, B. Knoch, M. Muller, S. Kersten, Peroxisome proliferator-activated receptor alpha target genes, PPAR Res 2010 (2010).
[6] G. Krey, O. Braissant, F. L'Horset, E. Kalkhoven, M. Perroud, M.G. Parker, W. Wahli, Fatty acids, eicosanoids, and hypolipidemic agents identified as ligands of peroxisome proliferator-activated receptors by coactivator-dependent receptor ligand assay, Mol. Endocrinol. 11 (6) (1997) 779–791.
[7] D.P. Oswal, M. Balanarasimha, J.K. Loyer, S. Bedi, F.L. Soman, S.D. Rider Jr., H.A. Hostetler, Divergence between human and murine peroxisome proliferator-activated receptor alpha ligand specificities, J. Lipid Res. 54 (9) (2013) 2354–2365.
[8] Y. Guo, R.A. Jolly, B.W. Halstead, T.K. Baker, J.P. Stutz, M. Huffman, J.N. Calley, A. West, H. Gao, G.H. Searfoss, et al., Underlying mechanisms of pharmacology and toxicity of a novel PPAR agonist revealed using rodent and canine hepatocytes, Toxicol. Sci. 96 (2) (2007) 294–309.
[9] M. Rakhshandehroo, G. Hooiveld, M. Muller, S. Kersten, Comparative analysis of gene regulation by the transcription factor PPARalpha between mouse and human, PLoS One 4 (8) (2009) e6796.
[10] M.T. Bility, J.T. Thompson, R.H. McKee, R.M. David, J.H. Butala, Vanden Heuvel JP, Peters JM, Activation of mouse and human peroxisome proliferator-activated receptors (PPARs) by phthalate monoesters, Toxicol. Sci. 82 (1) (2004) 170–182.
[11] H. Keller, P.R. Devchand, M. Perroud, W. Wahli, PPAR alpha structure–function relationships derived from species-specific differences in responsiveness to hypolipidemic agents, Biol. Chem. 378 (7) (1997) 651–655.
[12] F.J. Gonzalez, Y.M. Shah, PPARalpha: mechanism of species differences and hepatocarcinogenesis of peroxisome proliferators, Toxicology 246 (1) (2008) 2–8.
[13] Y.M. Shah, K. Morimura, Q. Yang, T. Tanabe, M. Takagi, F.J. Gonzalez, Peroxisome proliferator-activated receptor alpha regulates a microRNA-mediated signaling cascade responsible for hepatocellular proliferation, Mol. Cell. Biol. 27 (12) (2007) 4238–4247.
[14] S. Bosgra, W. Mennes, W. Seinen, Proceedings in uncovering the mechanism behind peroxisome proliferator-induced hepatocarcinogenesis, Toxicology 206 (3) (2005) 309–323.
[15] J.E. Klaunig, M.A. Babich, K.P. Baetcke, J.C. Cook, J.C. Corton, R.M. David, J.G. DeLuca, D.Y. Lai, R.H. McKee, J.M. Peters, et al., PPARalpha agonist-induced rodent tumors: modes of action and human relevance, Crit. Rev. Toxicol. 33 (6) (2003) 655–780.
[16] C. Cheung, T.E. Akiyama, J.M. Ward, C.J. Nicol, L. Feigenbaum, C. Vinson, F.J. Gonzalez, Diminished hepatocellular proliferation in mice humanized for the nuclear receptor peroxisome proliferator-activated receptor alpha, Cancer Res. 64 (11) (2004) 3849–3854.
[17] K. Morimura, C. Cheung, J.M. Ward, J.K. Reddy, F.J. Gonzalez, Differential susceptibility of mice humanized for peroxisome proliferator-activated receptor alpha to Wy-14,643-induced liver tumorigenesis, Carcinogenesis 27 (5) (2006) 1074–1080.
[18] T. Sher, H.F. Yi, O.W. McBride, F.J. Gonzalez, cDNA cloning, chromosomal mapping, and functional characterization of the human peroxisome proliferator activated receptor, Biochemistry 32 (21) (1993) 5598–5604.
[19] M.H. Hsu, C.N. Palmer, K.J. Griffin, E.F. Johnson, A single amino acid change in the mouse peroxisome proliferator-activated receptor alpha alters transcriptional responses to peroxisome proliferators, Mol. Pharmacol. 48 (3) (1995) 559–567.
[20] I. Takada, R.T. Yu, H.E. Xu, M.H. Lambert, V.G. Montana, S.A. Kliewer, R.M. Evans, K. Umesono, Alteration of a single amino acid in peroxisome proliferator-activated receptor-alpha (PPAR alpha) generates a PPAR delta phenotype, Mol. Endocrinol. 14 (5) (2000) 733–740.
[21] W.F. van Gunsteren, B.S.R. Eising, A.A. Hünenberger, P.H. Krüger, P. Mark, A.E. Scott, W.R.P.I.G. Tironi, Biomolecular Simulation: The GROMOS96 Manual and User Guide, Vdf Hochschulverlag AG an der ETH Zürich, Zürich, Switzerland, 1996.
[22] O. Trott, A.J. Olson, AutoDock Vina: improving the speed and accuracy of docking with a new scoring function, efficient optimization, and multithreading, J. Comput. Chem. 31 (2) (2010) 455–461.
[23] A.C. Wallace, R.A. Laskowski, J.M. Thornton, LIGPLOT: a program to generate schematic diagrams of protein–ligand interactions, Protein Eng. 8 (2) (1995) 127–134.
[24] J.D. Durrant, C.A. de Oliveira, J.A. McCammon, POVME: an algorithm for measuring binding-pocket volumes, J. Mol. Graph. Model. 29 (2011) 773–776.
[25] W. Humphrey, A. Dalke, K. Schulten, VMD: visual molecular dynamics, J. Mol. Graph. 14 (1996) 33–38.
[26] H.A. Hostetler, H. Huang, A.B. Kier, F. Schroeder, Glucose directly links to lipid metabolism through high affinity interaction with peroxisome proliferator-activated receptor alpha, J. Biol. Chem. 283 (4) (2008) 2246–2254.
[27] H.A. Hostetler, A.D. Petrescu, A.B. Kier, F. Schroeder, Peroxisome proliferator-activated receptor alpha interacts with high affinity and is conformationally responsive to endogenous ligands, J. Biol. Chem. 280 (19) (2005) 18667–18682.
[28] N. Sreerama, R.W. Woody, Estimation of protein secondary structure from circular dichroism spectra: comparison of CONTIN, SELCON, and CDSSTR methods with an expanded reference set, Anal. Biochem. 287 (2) (2000) 252–260.
[29] J.B. Kim, H.M. Wright, M. Wright, B.M. Spiegelman, ADD1/SREBP1 activates PPARgamma through the production of endogenous ligand, Proc. Natl. Acad. Sci. U. S. A. 95 (8) (1998) 4333–4337.
[30] A.A. Spector, J.C. Hoak, An improved method for the addition of long-chain free fatty acid to protein solutions, Anal. Biochem. 32 (2) (1969) 297–302.
[31] T. Nakagawa, N. Kurita, S. Kozakai, S. Iwabuchi, Y. Yamaguchi, M. Hayakawa, Y. Ito, T. Aoyama, T. Nakajima, Molecular mechanics and molecular orbital simulations on specific interactions between peroxisome proliferator-activated receptor PPARalpha and plasticizer, J. Mol. Graph. Model. 27 (1) (2008) 45–58.
[32] H. Reginald, Garrett CMG: Biochemistry, 5th ed., Brooks/Cole, Cengage Learning, 2013.
[33] C. Tanford, The Hydrophobic Effect: Formation of Micelles and Biological Membranes, 2nd ed., John Wiley and Sons, Inc., New York, 1979.
[34] H. Miyachi, H. Uchiki, Analysis of the critical structural determinant(s) of species-selective peroxisome proliferator-activated receptor alpha (PPAR alpha)-activation by phenylpropanoic acid-type PPAR alpha agonists, Bioorg. Med. Chem. Lett. 13 (19) (2003) 3145–3149.
[35] A.D. Petrescu, R. Hertz, J. Bar-Tana, F. Schroeder, A.B. Kier, Ligand specificity and conformational dependence of the hepatic nuclear factor-4a (HNFa), J. Biol. Chem. 277 (27) (2002) 23988–23999.
[36] W. Yassine, N. Taib, S. Federman, A. Milochau, S. Castano, W. Sbi, C. Manigand, M. Laguerre, B. Desbat, R. Oda, et al., Reversible transition between alpha-helix and beta-sheet conformation of a transmembrane domain, Biochim. Biophys. Acta 1788 (9) (2009) 1722–1730.
[37] H. Uchiki, H. Miyachi, Molecular modeling study of species-selective peroxisome proliferator-activated receptor (PPAR) alpha agonist; possible mechanism(s) of human PPARalpha selectivity of an alpha-substituted phenylpropanoic acid derivative (KCL), Chem. Pharm. Bull. (Tokyo) 52 (3) (2004) 365–367.
[38] M. Nagasawa, T. Ide, M. Suzuki, M. Tsunoda, Y. Akasaka, T. Okazaki, T. Mochizuki, K. Murakami, Pharmacological characterization of a human-specific peroxisome proliferater-activated receptor alpha (PPARalpha) agonist in dogs, Biochem. Pharmacol. 67 (11) (2004) 2057–2069.
[39] H. Escriva, F. Delaunay, V. Laudet, Ligand binding and nuclear receptor evolution, Bioessays 22 (8) (2000) 717–727.
[40] H. Escriva, R. Safi, C. Hanni, M.C. Langlois, P. Saumitou-Laprade, D. Stehelin, A. Capron, R. Pierce, V. Laudet, Ligand binding was acquired during evolution of nuclear receptors, Proc. Natl. Acad. Sci. U. S. A. 94 (13) (1997) 6803–6808.
[41] V. Laudet, Evolution of the nuclear receptor superfamily: early diversification from an ancestral orphan receptor, J. Mol. Endocrinol. 19 (3) (1997) 207–226.